Core-Shell Method of Synthesis, Characterizations, and ac Conductivity Studies of Polyaniline/n-TiO_2 Composites

Aashis S. Roy,[1] Koppalkar R. Anilkumar,[2] M. V. N Ambika Prasad[1]

[1]*Polymer Research Laboratory, Department of Materials Science, Gulbarga University, Gulbarga, Karnataka, India*
[2]*Materials Research Centre, Department of Physics, S.S. Margol College, Shahabad, Gulbarga, Karnataka, India*

Received 12 July 2010; accepted 9 November 2010
DOI 10.1002/app.33730
Published online 23 February 2011 in Wiley Online Library (wileyonlinelibrary.com).

ABSTRACT: Polyaniline/nano-titanium dioxide composites (PANI/n-TiO_2) were prepared using α-dextrose as surfactant and ammonium per sulfate as oxidant. The PANI/n-TiO_2 composite is characterized by Fourier transform infrared spectra and confirmed the presence of benzenoid and qunoide ring structures and also formation of free ions. The transmission electron microscopy study reveals that the size of TiO_2 is in the order of 7 nm where as the composite size is of the order of 13 nm; further, it is observed that the TiO_2 particles are intercalated to form a core shell of PANI. The X-ray diffraction (XRD) studies show that the monoclinic structure of the composites. ac Conductivity, permittivity, and tangent loss studies on these samples suggest that these composites may be well suited for gas sensor. © 2011 Wiley Periodicals, Inc. J Appl Polym Sci 121: 675–680, 2011

Key words: polyaniline; nano-TiO_2; α-dextrose; permittivity and conductivity

INTRODUCTION

In recent years, conducting polymer composites have drawn considerable interest because of their numerous applications in various electrical and electronic devices. In most of these applications, the main objective is to obtain a sufficient level of conductivity in the material. Lately, it has been found that these composites can exhibit some novel properties such as positive temperature coefficient of resistance, photosensitivity, etc.[1–6]

Another interesting type of polymer nanocomposites is that in which the inorganic material represents the nanometric phase. In this way, a great number of nanocomposites between conducting polymers and nanoparticles of different oxides as CuO, Fe_2O_3, and SnO_2 have been reported.[7–15] Several reports involving the synthesis and characterization of different polypyrrole or polyaniline (PANI)/TiO_2 hybrids have been described aiming to obtain materials that find applications in electrochromic devices, nonlinear optical systems, photoelectrochemical devices, etc.[16–20]

TiO_2/conducting polymer hybrids have been prepared by chemical polymerization of the monomer in a dispersion, which contains the oxide nanoparticles. The synthesis conditions are fundamental to control the properties of the resulting materials like size and shape of the oxide particles, degree of the dispersion, kind of interaction, and interface between the organic and the inorganic phases, have direct influence on properties like conductivity, piezoresistivity, photocurrent, etc.[16,21]

It is felt that the origin of these effects lies in the mechanism of charge transport process present in these materials. The charge transport process in conducting polymer composites is quite complex, often exhibiting nonlinear conduction characteristics which give rise to a number of novel effects. The authors in this article report characterization and the electrical properties of core-shell composites prepared by using α-dextrose as a surfactant.

EXPERIMENTAL

All chemicals used were analytical grade. The monomer aniline was doubly distilled before use. Ammonium persulfate ($(NH_4)_2S_2O_8$) and hydrochloric acid (HCl) were procured and were used as received.

Correspondence to: M. V. N. A. Prasad (prasad1_amb@rediffmail.com).

Contract grant sponsor: Department of Science and Technology (DST); contract grant number: SR/S2/CMP-20/2007.

Preparation of titanium dioxide

A two step sol–gel preparation method is used to synthesize nano-titanium dioxide (n-TiO_2) and is described as follows:

In the first step, 160 mL of 0.1*N* titanium nitrate hydrated [$(TiO_2)N_2O_5{\cdot}6H_2O$] and 480 mL of 0.1*N* citric acid are taken. To this mixture, ammonia is added with constant stirring using magnetic stirrer for 5–6 h. The purpose of adding ammonia is to maintain the pH = 4. Finally, a gel is formed.

In the second step, the saturated solution of alpha dextrose is added to above said gel and stirred for 2 h at 120°C, which turns to a spongy type solid residue. This spongy gel is ignited at a temperature of about 300°C for 1 h. Finally, about 5 gm of fine graded TiO_2 nanoparticles are formed.

Preparation of composite

Aniline/HCl taken in 1 : 2 and [(TiO2) $N_2O_5{\cdot}6H_2O$]/ citric acid are taken in 1 : 3 ratio and are stirred thoroughly for 1 h at 25°C. To this mixture, $(NH_4)_2S_2O_8$ and α-dextrose are added with constant stirring using magnetic stirrer at 70°C for 5–6 h. Finally, a green gel is obtained. The gel is further refluxed with 0.1*N* HCl to enhance the protonation processes, and finally, it is vigorously washed with distilled water to remove the excess α-dextrose and citric acid from the composite (Fig. 1). The composites are prepared in different weight percentage of TiO_2 in PANI (10, 20, 30, 40, and 50 wt %).

The pellets of 10-mm diameter are prepared with thickness varying up to 2 mm by applying pressure of 10 Tons in a UTM–40 (40 Ton Universal testing machine). For temperature-dependent conductivity and sensor studies, the pellets are coated with silver paste on either side of the surfaces. The copper electrodes are placed on each of the surface to obtain better contacts.

EXPERIMENTAL TECHNIQUES

X-ray diffraction phase identification was carried out by X-ray powder diffraction at ambient temperature. A Shintag X1 diffractometer with Cu K_α (1.54 Å) radiation in θ–θ configuration was used. The patterns were recorded in the 2–70° range at 0.05° step size using 3-s acquisition time per step. The mean particle size was calculated using the Debye–Scherer equation $D = K\lambda/\beta\text{Cos }\theta$, in which *K* is a constant equal to 0.9, λ is the wavelength of the Cu K_α radiation, β is the full-width half-maxima of the diffraction peak in radiant, and θ is the Bragg's angle of (311) plane.

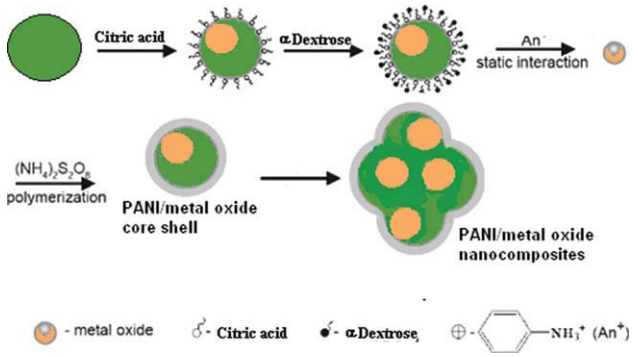

Figure 1 Schematic illustration for the formation of well-controlled core/shell metal oxides/PANI nanocomposites and PANI capsules. A double-surfactant layer (CA-Dextrose) was formed on the metal oxide core surface. The polymerization of aniline was successfully initiated, propagated, and terminated on the surface of the metal oxide core. [Color figure can be viewed in the online issue, which is available at wileyonlinelibrary.com.]

Infrared spectroscopy

The IR spectra of all the samples are recorded on Perkin Elmer (model 783) IR spectrometer in KBr medium at room temperature. For recording IR spectra, powders are mixed with KBr in the ratio 1 : 25 by weight to ensure uniform dispersion. The mixed powders are pressed in a cylindrical dye to obtain clean disks of ~ 1 mm thickness.

Transmission electron microscopy

The particle morphology of PANI and its composites sintered in the form of pellets are investigated using transmission electron microscopy (TEM) (JEOL-2010).

RESULTS AND DISCUSSIONS

X-ray diffraction

Figure 2(a–c) shows that the X-ray diffraction (XRD) of the PANI, n-TiO_2 particles, and PANI/nano-TiO_2 composite with 50 wt % of TiO_2 in PANI. Figure 2(a) reveals that the PANI has amorphous in nature. A maximum peak is around 26° for PANI, which may be assigned to the scattering from PANI chains at interplanar spacing.[22] When $(NH_4)_2S_2O_8$ is added to the reaction system, polymerization proceeds initially on the surface of n-TiO_2 particles. After PANI encapsulates n-TiO_2 particles, due to the restrictive effect of the surface of nano-TiO_2 particles, the crystalline behavior of PANI is hampered. Therefore, the degree of crystallinity of PANI increases and the diffraction peaks emerged with peaks TiO_2 and hence cannot be distinguished. By comparing with the curves of pure TiO_2 and PANI/n-TiO_2 composite, it is obtained that the PANI deposited on the surface

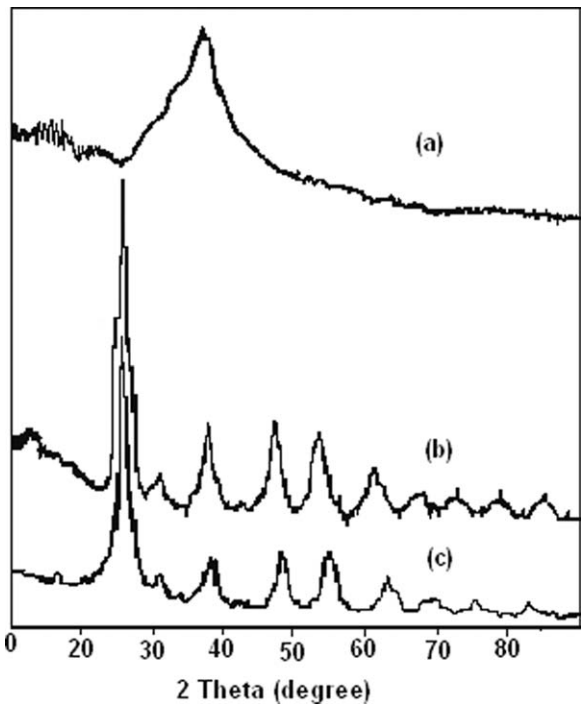

Figure 2 The XRD of (a) polyaniline, (b) n-TiO_2 particles, and (c) polyaniline/n-TiO_2 composite with 50 wt % of TiO_2 in polyaniline.

of n-TiO_2 particles has no effect on crystallization performance of n-TiO_2 particles.

It is seen from Figure 2(b,c) that the monoclinic peak of TiO_2 indicates the crystalline nature of the n-TiO_2 and PANI/n-TiO_2 composite. By comparing the XRD pattern of PANI/n-TiO_2 composite with that of TiO_2, the prominent peaks corresponding to 2θ = 25.61°, 38.12°, 47.53°, and 54.03° are due to (110), (101), (111), and (211) planes which indicates the presence of TiO_2 in PANI [JCPDS file no. 21-1276]. By comparing the XRD patterns of pure PANI with its composites, it is observed that TiO_2 has retained its structure even though it is dispersed in PANI after polymerization reaction.

Infrared spectroscopy

Figure 3(a) shows Fourier transform infrared spectra (FTIR) spectra of pure TiO_2. It shows a broadband around 634 and 3419 cm^{-1}, which corresponds to Ti—O—Ti and O—H stretching frequencies. The characteristic vibrations of PANI are known to be in the region of 1000–1500 cm^{-1}. The IR spectra of PANI and PANI/n-TiO_2 [Fig. 3(b,c)] show vibrations around 503, 808, 1133, 1294, 1491, and 1581 cm^{-1}. The bands at 503 and 808 cm^{-1} are due to C—H out-of-plane bending vibration and para-disubstituted aromatic rings, respectively. A band appearing near 1294 cm^{-1} represents the C—N stretching vibration. The C—H in the plane bending vibration occurs at 1133 cm^{-1}. The presence of the two bands in the range of 1450–1600 cm^{-1} is assigned to the nonsymmetric C_6 ring stretching modes. The higher frequency vibration at 1581 cm^{-1} has a major contribution from the quinoid rings, whereas the lower frequency mode at 1491 cm^{-1} depicts the presence of benzenoid ring units. The broadband observed at 3280–3500 cm^{-1} is due to the N—H stretching of aromatic amines and at 2500–3000 cm^{-1} is due to aromatic C—H stretching vibrations. The FTIR results confirm the formation of PANI/n-TiO_2 composite.

Transmission electron microscopy

Figure 4(a,b) shows TEM images of PANI and PANI/n-TiO_2 nanoparticles obtained of about average size 7 nm and 13 nm, respectively. The TEM images of the n-TiO_2 and PANI/n-TiO_2 composite show the granular structures. The surface to volume ratio of n-TiO_2 particles decreases the size of composite from bulk to nano. This may be the reason why the particle size decreases with an increase in the concentration of the composite. The PANI fibers provide strength and stiffness to the TiO_2 composite, whereas the PANI matrix acts as a binder that distributes external load to the fibers. In addition to increasing the rigidity of the polymer matrix, the particles are added to modify rheological property. The conformational energy map of PANI matrix macromolecules displays a very rigid and extended structure. This may be attributed to the formation of intra residue hydrogen bonds between the molecules, resulting in a zig-zag-shaped structure.

Conductivity measurement

The frequency-dependent ac conductivity of PANI and PANI/n-TiO_2 composites are studied in the

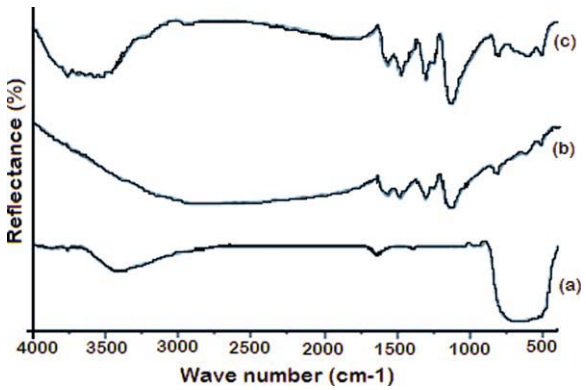

Figure 3 FTIR spectra of (a) TiO_2, (b) PANI, and (c) PANI/TiO_2 nanocomposites. [Color figure can be viewed in the online issue, which is available at wileyonlinelibrary.com.]

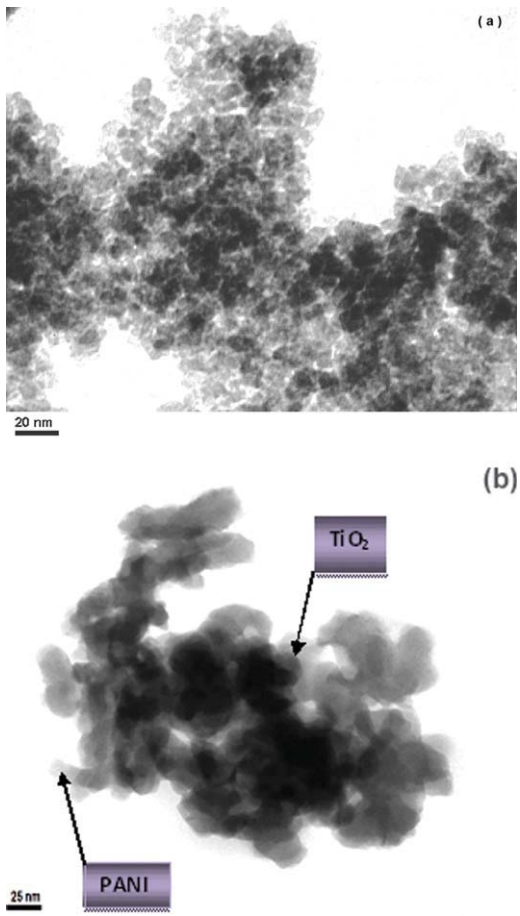

Figure 4 (a) The TEM image of pure n-TiO_2 and (b) the TEM image of PANI/n-TiO_2 composites. [Color figure can be viewed in the online issue, which is available at wileyonlinelibrary.com.]

frequency range 10^2 to 10^6 Hz at room temperature using Hioki LCR Q meter.

ac Conductivity

Figure 5 shows that the variation of σ_{ac} versus logarithmic of frequency for various weight percentage of n-TiO_2 in PANI matrix. Among all composites, 30 and 40 wt % show higher conductivity of about 0.65 S/cm and 0.5 S/cm at frequency of 10^6 Hz, respectively. This is due to the space charge polarization and electrode polarization, i.e., positive charges are displaced along the field and negative charges shift in the opposite direction creates an internal electric field which partly compensates the external field inside the composites. However, 10, 20, and 50 wt % of PANI/n-TiO_2 composites shows conductivity due to dipole polarization where the rotation of dipoles between two equivalent equilibrium positions is involved. It is the spontaneous alignment of dipoles in one of the equilibrium positions that give rise to the nonlinear polarization behavior of these composites. Further, conductivity for 100 wt % is due to the electron polarization and thus shows very low conductivity among all the composites.

This behavior of 30 and 40 wt % PANI/n-TiO_2 composites obeys the universal power law, $\sigma(\omega) = \sigma_0 + A\omega^n$ (the solid line is the fit to the expression), where σ_0 is the dc conductivity (frequency independent plateau in the low frequency region), A is the pre-exponential factor, and n is the fractional exponent between 0 and 1. On crystallization, the conductivity spectrum remains similar as that of the PANI except dispersion in the low frequency region, where the deviation from σ_{dc} (plateau region) is more prominent. The deviation from σ_{dc} (plateau region) value in the conductivity spectrum (in the low frequency region) is due to the electrode polarization effect. The values of σ_0, A, and n were obtained by fitting the $\sigma(\omega)$ to $\sigma(\omega) = \sigma_0 + A\omega^n$. The overall behavior of σ_{ac} follows the universal dynamic response,[23] which has widely been observed in disordered materials like ionically conducting glasses,[24] conducting polymers, and also doped crystalline solids,[25,26] and is generally believed to be reflected in the mechanism of charge transport behavior of charge carriers.

Figure 6 shows that the variation of σ_{ac} for various weight percentage of TiO_2 in PANI matrix as a function of frequencies (10, 100, and 1000 kHz).

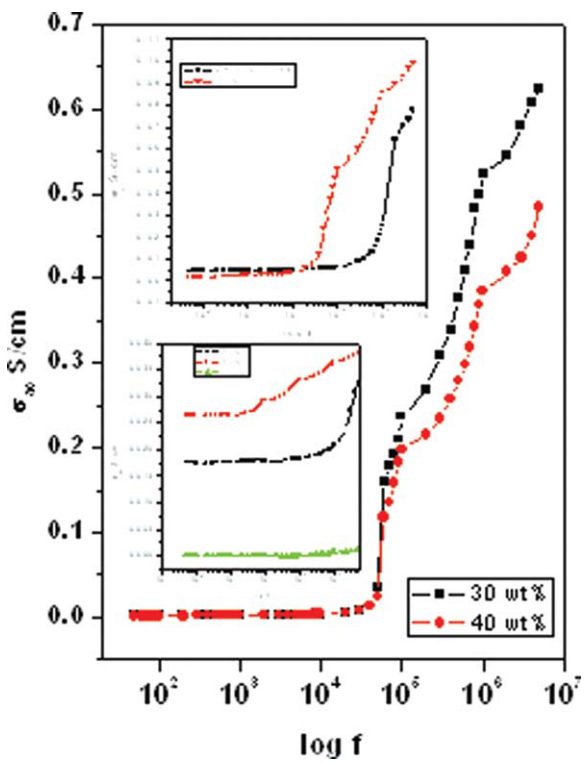

Figure 5 The variation of σ_{ac} versus logarithmic of frequency for various weight percentage of n-TiO_2 in PANI matrix. [Color figure can be viewed in the online issue, which is available at wileyonlinelibrary.com.]

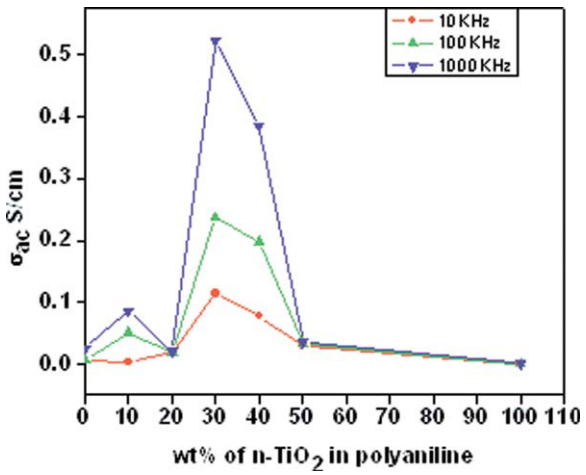

Figure 6 The variation of σ_{ac} various weight percentage of TiO_2 in PANI matrix as a function of frequencies (10, 100, and 1000 kHz). [Color figure can be viewed in the online issue, which is available at wileyonlinelibrary.com.]

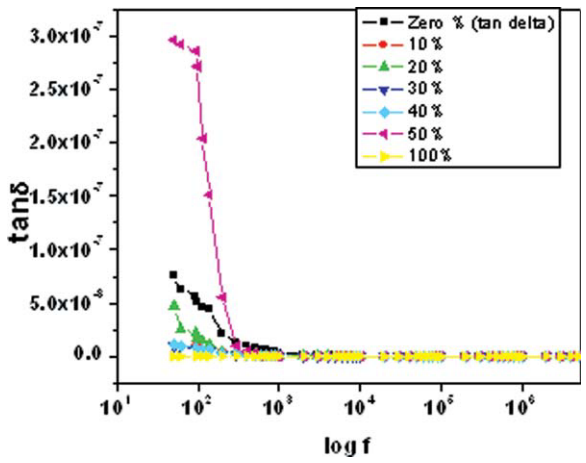

Figure 8 The dielectric tangent loss (tan δ) as a function of frequency for pure PANI, n-TiO_2, and PANI/n-TiO_2 for the different wt %. [Color figure can be viewed in the online issue, which is available at wileyonlinelibrary.com.]

Among all the composites, 30 wt % of PANI/n-TiO_2 shows the highest conductivity of about 0.65 S/cm at 1000 kHz, and for pure PANI, n-TiO_2 and other composites of 10, 20, 40, and 50 wt % show the low conductivity.

Figure 7 shows the variation of dielectric constant (ε′) with frequency for different wt % of n-TiO_2 in PANI at room temperature. It is found that in all these composites, as frequency increases, dielectric constant decreases up to the frequency range of 10^3 Hz and after that it remains constant for further increasing in frequency. The strong frequency dispersion of permittivity is observed in the low frequency region followed by a nearly frequency independent behavior above 10 kHz. It is observed that Debye type relaxation mechanism is responsible for higher value of 0, 20, and 50 wt % PANI/n-TiO_2 composites.

Figure 8 shows that the dielectric tangent loss (tan δ) as a function of frequency for pure PANI, n-TiO_2, and PANI/n-TiO_2 for the different wt %. It is observed that the dielectric loss decreases as a function of frequency. PANI and PANI/n-TiO_2 exhibit small value of dielectric loss at higher frequencies, which suggests that these materials are lossless materials at frequencies beyond 10^6 Hz. The observed behavior is in consistent with the conductivity and dielectric constant results in these composites.

Figure 9 shows complex plane impedance cole–cole plots for different weight percentage of PANI and PANI/n-TiO_2 composites. It is observed through the graph that the complex impedance plots

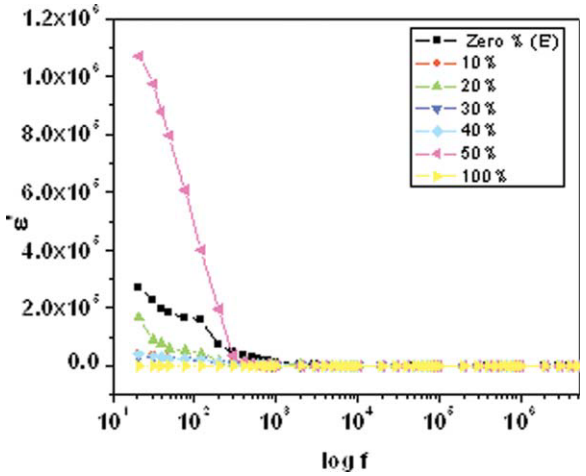

Figure 7 The variation of dielectric constant (ε′) with frequency for different wt % of n-TiO_2 in PANI at room temperature. [Color figure can be viewed in the online issue, which is available at wileyonlinelibrary.com.]

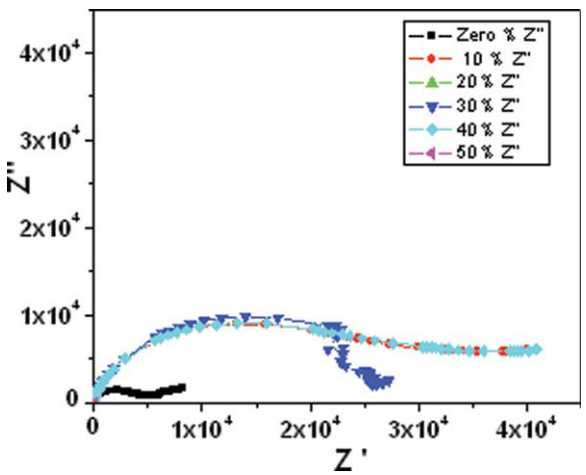

Figure 9 Complex plane impedance cole–cole plots for different weight percentage of polyaniline and PANI/n-TiO_2 composites. [Color figure can be viewed in the online issue, which is available at wileyonlinelibrary.com.]

show a single semicircular arc passing through the origin. This arc is due to the electrical properties of the parallel combination of bulk grain resistance and bulk gain capacitance of PANI and PANI/n-TiO_2 composite, and the other semicircles are not completely resolved at higher frequency region. This indicates that the resistance of grain boundary is very high in comparison with the bulk. Thus, grains dominate the conductivity of the sample, and the role of grain boundary is negligible in conduction at higher frequencies. Thus, the intercept made by the semicircle at the high frequency end corresponds to the resistance offered by bulk grain, and the intercept due to low frequency arc corresponds to the combined resistance of grain boundaries.[27]

CONCLUSIONS

PANI/n-TiO_2 composites are successfully prepared using core-shell method. FTIR conforms the formation of PANI/n-TiO_2 composites and also formation of free ions. The TEM study of TiO_2 reveals that the size is of the order of 9 nm where as the composite size is of the order of 13 nm. The XRD studies supports the size around 7 nm, and it is found that the composite is of high melting point unlike other PANI/metal oxide composite. ac Conductivity, permittivity, and tangent loss studies on these samples suggest that the materials may be well suited for gas sensor.

References

1. Epstein, A. J.; MacDiarmid, A. G. Makromol Chem Macromol Symp 1991, 51, 217.
2. Heinze, J. Top Curr Chem 1990, 152, 2.
3. Yang, Y.; Heeger, A. J. Appl Phys Lett 1994, 64, 1245.
4. Unde, S.; Ganu, J.; Radhakrishnan, S. Adv Mater Opt Electron 1996, 6, 151.
5. Wada, Y. In Electronic Properties of Polymers; Mort, J., Pfister, G., Eds.; Wiley: New York, 1982; p 109.
6. Nalwa, H. S. Ferroelectric Polymers; Marcel Dekker: New York, 1995; p 1183.
7. Wang, T. T.; Herbert, J. M.; Glass, A. M. The Applications of Ferroelectric Polymers; Blackie: Glasgow, CA, 1988; Vol. 110, pp 21–36.
8. Maeda, S.; Armes, S. P. Chem Mater 1995, 7, 171.
9. Tang, B. Z.; Geng, Y. H.; Lam, J. W. Y.; Li, B. S.; Jing, X. B.; Wang, X. H.; Wang, F. S.; Pakhomov, A. B.; Zhang, X. X. Chem Mater 1999, 11, 1581.
10. Suri, K.; Annapoorni, S.; Sarkar, A. K.; Tandon, R. P.; Sens Actuators B 2002, 81, 277.
11. Hao, Y.; Yang, M.; Yu, C.; Cai, S.; Liu, M.; Fan, L.; Li, Y. Solar Energy Mater Solar Cells 1998, 56, 75.
12. Feng, W.; Sun, E.; Fujii, A.; Wu, H.; Nihara, K.; Yoshino, K. Bull Chem Soc Jpn 2000, 73, 2627.
13. Su, S.-J.; Kuramoto, N. Synth Met 2000, 114, 146.
14. Gurunathan, K.; Trivedi, D. C. Mater Lett 2000, 45, 262.
15. Xia, H.; Wang, Q. Chem Mater 2002, 14, 2158.
16. Nogueira, A. F.; Micaroni, L.; Gazotti, W. A.; De-Paoli, M. A. Electrochem Commun 1999, 1, 262.
17. Murakoshi, K.; Kogure, R.; Wada, Y.; Yanagida, S. Chem Lett 1997, 5, 471.
18. Murakoshi, K.; Kogure, R.; Wada, Y.; Yanagida, S. Solar Energy Mater Solar Cells 1998, 55, 113.
19. Wang, G.; Chen, H.; Zhang, H.; Yuan, C.; Lu, Z.; Wang, G.; Yang, W. Appl Surf Sci 1998, 135, 97.
20. Kobayashi, N.; Teshima, K.; Hirohashi, R. J Mater Chem 1998, 8, 497.
21. Avvaru, N. R.; Tacconi, N. R.; Rajeshwar, K. Analyst 1998, 123, 113.
22. Xia, H. S.; Wang, Q. Chem Mater 2002, 14, 2158.
23. Jonscher, A. K. Dielectric Relaxation in Solids; Chelsea Dielectric Press: London, 1983.
24. Elliott, S. R. Solid State Ionics 1988, 27, 131.
25. Leon, C.; Lucıa, M. L.; Santamarıa, J. Phys Rev 1997, B55, 882.
26. Leon, C.; Lucıa, M. L.; Santamarıa, J.; Parsı, M. A.; Sanz, J.; Varez, A. Phys Rev 1996, B54, 184.
27. Dyre, J. C. J Appl Phys 1988, 64, 2456.